A semi-global chemistry mechanism for low-pressure oxygen-methane combustion

By D. Brouzet AND D. Passiatore

1. Motivation and objectives

One of the objectives of the Stanford Predictive Science Academic Alliance Program (PSAAP) III Center is to predict the reliability of laser ignition in a rocket combustor fueled by methane and oxygen reactants at in-flight conditions. This prediction can be achieved through multifidelity ensembles of numerical simulations running on exascale-class, heterogeneous supercomputers (CPUs+GPUs). As part of the continuous effort to improve the numerical methods and physical models implemented in the Hypersonics Task-based Research (HTR) solver (Di Renzo *et al.* 2020), developed as part of the Stanford PSAAP-II and PSAAP-III Centers, the work presented in this brief focuses on the chemistry modeling in the context of the rocket combustor ignition process.

Detailed kinetic schemes such as GRI 3.0 (Smith *et al.* 1999) for methane combustion or AramcoMech1.3 (Metcalfe *et al.* 2013) for small hydrocarbon fuels can include up to hundreds of species and thousands of reactions. The inherently high computational cost associated with the transport of a large amount of species usually results in computationally unaffordable 3D large-eddy simulations (LESs). To make 3D simulations of reacting flows computationally affordable, detailed chemistry mechanisms need to be reduced to smaller mechanisms. This can be achieved by eliminating unimportant species and reactions, for instance through sensitivity analysis (Tomlin *et al.* 1992), path-flux analysis (Sun *et al.* 2010) or graph-based methods (Lu & Law 2005; Pepiot-Desjardins & Pitsch 2008) to create a skeletal mechanism.

Two aspects related to the PSAAP-III project give us incentives to reduce even further chemistry mechanisms. First, considering ensemble simulations necessary for the prediction of ignition probability maps or for uncertainty quantification purposes, hundreds if not thousands of numerical simulations will be required. Computational costs must be reduced to a minimum in this situation. Furthermore, the excessive memory usage necessary to handle complex chemistries could be detrimental to the performance of GPU-based computations. Reducing the number of transported species, and therefore memory usage, becomes paramount to reach the optimum compute-bound regime.

To the extreme limit where a full mechanism is reduced to one overall reaction, the reduced scheme is identified as global. An alternative is to keep a few important reactions. Such mechanisms are called semi-global and have been extensively used in the past two decades [e.g., Brewster *et al.* (1999); Andersen *et al.* (2009); Franzelli *et al.* (2012)]. While more recent methodologies, such as neural networks [e.g., An *et al.* (2020); Wan *et al.* (2020); Sharma *et al.* (2020)] or bottom-up construction approaches (Heberle *et al.* 2021), have been explored for low-cost chemistry modeling, these global and semi-global frameworks are attractive because of their simplicity of use and implementation.

In this brief, we present the development and assessment of a computationally efficient semi-global chemistry mechanism for modeling low-pressure oxygen-methane combustion.

We assess the newly devised mechanism, named BFERoxy, for a range of conditions and configurations relevant to in-flight ignition of rocket combustors.

2. Chemistry mechanisms

2.1. *Reference mechanisms*

For validation and comparison purposes, two mechanisms were used as references:

(1) GRI 3.0 (Smith *et al.* 1999), designed for methane combustion; 53 species and 325 reactions.

(2) A Foundational Fuel Chemistry Model (Tao *et al.* 2018) (FFCM), designed for oxygen-methane combustion; 12 species and 39 reactions.

GRI 3.0 is a well-established mechanism but is computationally expensive for 3D configurations. Therefore, GRI 3.0 is used as reference only in the 1D configurations presented in this study. Recently, a FFCM chemistry model was developed, targeting oxygen-methane combustion in rocket engines at high pressure. A branch mechanism for atmospheric conditions was obtained through private communication and was validated against GRI 3.0 at sub-atmospheric pressure conditions. This branch mechanism is used as reference for 2D and 3D configurations.

2.2. *Assessment of existing global and semi-global mechanisms*

As a first step, a set of semi-global and global mechanisms, either developed for air-methane or oxygen-methane combustion, are considered for modeling oxygen-methane combustion in the PSAAP rocket combustor:

(1) BFER mechanism (Franzelli *et al.* 2012), designed for air-methane combustion; five species and two reactions.

(2) One-step mechanism (CERFACS 2023), designed for air-methane combustion; four species and one reaction.

(3) Westbrook-Dryer (WD) mechanism modified by Andersen *et al.* (2009), designed for oxygen-methane combustion; five species and three reactions.

Test cases in 1D premixed laminar flame configurations are performed to assess if main flame parameters such as the laminar flame speed S_L and the thermal flame thickness $\delta_{th} = (T_b - T_u)/\max(\partial T/\partial x)$ are correctly predicted. The b and u subscripts denote the burnt and fresh states, respectively. All 1D simulations in the present study are performed with the open-source code Cantera (Goodwin *et al.* 2018). Results are shown in Figure 1 for low-pressure conditions at $p = 30$ kPa and an unburnt gas temperature of $T_u = 300$ K. The reference results obtained with GRI 3.0 are illustrated by the solid line. Globally, S_L is grossly overpredicted by the reduced mechanisms, especially by the BFER and WD models. This high S_L is caused by a high reactivity, since in a 1D laminar flame we have

$$S_L = -\frac{1}{\rho_u Y_{F,u}} \int_{-\infty}^{\infty} \dot{\omega}_F dx \ , \tag{2.1}$$

where $\dot{\omega}_F$ is the reaction rate of the fuel. The higher reaction rates predicted by the reduced mechanisms also lead to a thinner flame, as exemplified by the δ_{th} predictions in Figure 1. Overall, the reduced mechanisms yield unsatisfactory results that could lead to unphysical flame dynamics in the PSAAP combustor.

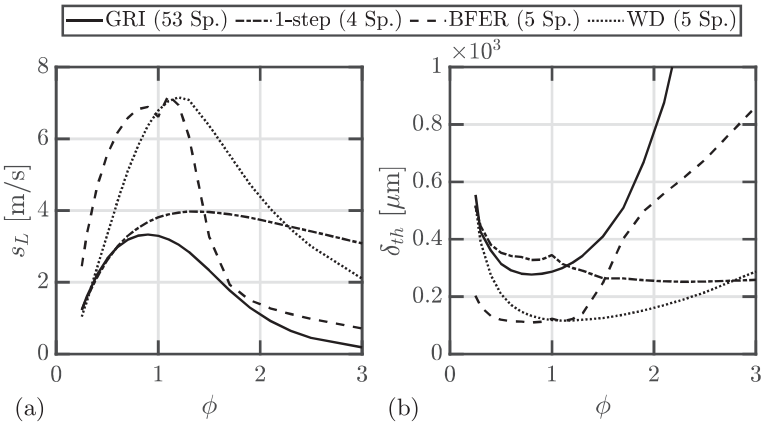

FIGURE 1. (a) Laminar flame speed and (b) thermal flame thickness of global/semi-global mechanisms found in the literature compared to the GRI 3.0 chemistry. The configurations are 1D premixed oxygen-methane laminar flames at 30 kPa and $T_u = 300$ K, in an equivalence ratio range of $0.25 < \phi < 3$.

2.3. *Development of BFERoxy*

Based on the results presented in the previous section, we have developed a semi-global mechanism for oxygen-methane combustion. Conditions relevant for in-flight, low-pressure, rocket ignition were targeted, i.e., 0.1 atm $< p <$ 1 atm, 200 K $< T_u <$ 500 K and $0.25 < \phi < 3$. We have used the framework of the BFER chemistry model (Franzelli 2011; Franzelli *et al.* 2012), which is composed of the following reactions

(a) $CH_4 + 1.5\ O_2 \rightarrow CO + 2\ H_2O$,
(b) $CO + 0.5\ O_2 \leftrightarrow CO_2$.

The first reaction models the combination of methane with radicals and the subsequent production of CO and H_2O. Then, a slow oxidation of CO into CO_2 occurs in the post-reaction zone, as modeled by the second reaction. The reaction rates are written in the classical Arrhenius form

$$k_{f,1} = A_1 f_1(\phi) T^{\beta_1} \exp\left(-\frac{E_1}{RT}\right) [CH_4]^{n_{CH4}} [O_2]^{n_{O2}}, \tag{2.2}$$

$$k_{f,2} = A_2 f_2(\phi) T^{\beta_2} \exp\left(-\frac{E_2}{RT}\right) [CO][O_2]^{0.5}, \tag{2.3}$$

where A is the pre-exponential coefficient, β is the temperature exponent, E is the activation energy, and R is the universal gas constant. The reaction order for species i is denoted by n_i, which is applied to the reactants' concentration in the methane oxidation reaction. Global or semi-global schemes guarantee proper flame predictions only for lean combustion and greatly overestimate the laminar flame speed in the rich regime. To overcome this problem, the Pre-Exponential Adjustment method, where the rate constants are allowed to vary with equivalence ratio ϕ, is being used. This adjustment is performed through the correction functions f_1 and f_2.

To identify the unknown parameters in Eqs. (2.2) and (2.3), 1D laminar premixed flame solutions are computed using the GRI 3.0 mechanism. Then, the parameters of the

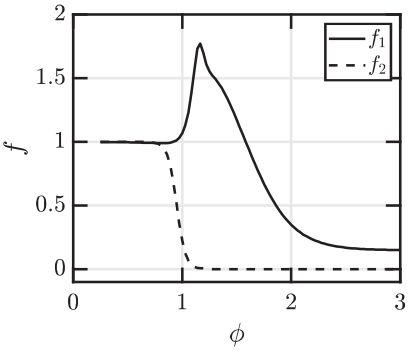

FIGURE 2. Correction functions f_1 and f_2 for the BFERoxy mechanism.

semi-global mechanism are altered to obtain the same laminar flame speed and thermal flame thickness. More specifically, the methodology is as follows:

(1) The pressure exponent α_P indicates how the laminar flame speed changes with the pressure conditions

$$S_L/S_{L,0} \propto (p/p_0)^{\alpha_P}, \tag{2.4}$$

where the subscript 0 denotes a reference condition, taken as $p_0 = 101$ kPa. Based on 1D flames in the range of conditions 10 kPa $< p <$ 1 atm, $0.5 < \phi < 2$ and 200 K $< T_u <$500 K, α_P is computed by performing a least-square regression on the laminar flame speed. Then, the reaction orders of the reactants are computed using the following relation

$$\alpha_P = (n_{\mathrm{CH4}} + n_{\mathrm{O2},1} - 2)/2. \tag{2.5}$$

With $\alpha_P = -0.05$, we obtain $n_{\mathrm{CH4}} = n_{\mathrm{O2}} = 0.95$, where it was assumed that both reaction orders were equal.

(2) The temperature exponent α_T indicates how the laminar flame speed changes with the temperature conditions

$$S_L/S_{L,0} \propto (T_u/T_{u,0})^{\alpha_T}. \tag{2.6}$$

In a similar procedure to the one performed in step (1), α_T was computed to be equal to 1.15. Usually, the β coefficients need to be adjusted to retrieve the S_L dependence on temperature. In the current study, it was found that the coefficients from the original BFER mechanism led to the correct temperature-dependent behavior with $\beta_1 = 0$ and $\beta_2 = 0.7$.

(3) Using a lean condition ($\phi = 0.7$), where the correction functions are unity, we find the correct pre-exponential coefficient A, while keeping the activation energy E_a from the original BFER mechanism.

(4) Finally, using 1D flame simulations with the newly devised mechanism at $p =$ 1 atm and $T_u = 300$ K, the correction functions f_1 and f_2 are tabulated to retrieve the S_L and δ_{th} variations as a function of the equivalence ratio from $\phi = 0.25$ to $\phi = 3$. The resulting coefficients are then fitted to well-devised analytical functions for ease of use. The correction functions are shown in Figure 2. At lean conditions, no correction is required. The correction for the first reaction increases to its maximum just above stoichiometry and then decreases to artificially decrease the reactivity for rich mixtures. The parameters of the new mechanism, named BFERoxy, are summarized in Tables 1 and 2 and Eqs. (2.7) and (2.8) below.

TABLE 1. Chemistry parameters for the BFERoxy mechanism. Units are mol, s, cm^3 and cal/mol.

	CH_4 oxidation	CO-CO_2 oxidation
Pre-exponential coefficient A	9.0E+13	2.0E+8
Temperature exponent β	0.0	0.7
Activation energy E	3.55E+4	1.2E+4
Reaction orders n	$n_{CH4} = n_{O2} = 0.95$	-

TABLE 2. Parameters for the correction functions.

	ϕ_{0j}	σ_{0j}	B_j	ϕ_{1j}	σ_{1j}	C_j	ϕ_{2j}	σ_{2j}	ϕ_{3j}	σ_{3j}
$j=1$	1.115	0.104	6.224	2.106	0.422	0.518	1.176	0.066	-	-
$j=2$	0.95	0.08	1.25E-5	1.3	0.04	4.35E-3	1.2	0.04	1.2	0.05

$$f_1(\phi) = \frac{2}{1 + \tanh\left(\frac{\phi_{01}-\phi)}{\sigma_{01}}\right) + C_1\left[1 + \tanh\left(\frac{\phi-\phi_{21}}{\sigma_{21}}\right)\right] + D_1\left[1 + \tanh\left(\frac{\phi-\phi_{31}}{\sigma_{31}}\right)\right]}, \quad (2.7)$$

$$f_2(\phi) = 0.5\left[1 + \tanh\left(\frac{\phi_{02}-\phi}{\sigma_{02}}\right)\right] + B_2\left[1 + \tanh\left(\frac{\phi-\phi_{12}}{\sigma_{12}}\right)\right] + C_2\left[1 + \tanh\left(\frac{\phi-\phi_{22}}{\sigma_{22}}\right)\right]\left[1 + \tanh\left(\frac{\phi_{32}-\phi}{\sigma_{32}}\right)\right]. \quad (2.8)$$

3. Results

In the following, we assess the performance of the newly devised BFERoxy mechanism in a variety of 1D, 2D and 3D configurations. Of note, we do not report any 0D reactor results of autoignition. In the context of the PSAAP-III project, the deposited laser kernel, which initializes the ignition, features extremely high temperatures, remaining above 3000 K even after 100 μs (see Section 3.4). At these temperatures, ignition is extremely fast, less than 1 μs according to 0D reactor calculations. Therefore, potential timescale errors introduced by chemistry modeling are negligible compared to the other physical mechanisms governing the ignition process (e.g., kernel convection, eddy turnover time) and the flame development.

3.1. *Laminar premixed flames*

Using a 1D laminar flame, we can assess the reproducibility of key quantities of interest. In addition to the laminar flame speed S_L and the thermal flame thickness δ_{th}, which were used for calibrating the mechanism parameters, the spatially integrated heat release $\dot{Q}_{tot}$, the adiabatic flame temperature T_{ad} and the species mass fraction in the burned gases are analyzed in the following. Results obtained with the GRI 3.0 and BFERoxy mechanisms are reported in Figure 3 for 1D premixed oxygen-methane laminar flames with $T_u = 300$ K, and both atmospheric and sub-atmospheric conditions. Additional results in the range 200 K $< T_u <$ 500 K (not shown) are consistent with the discussion below.

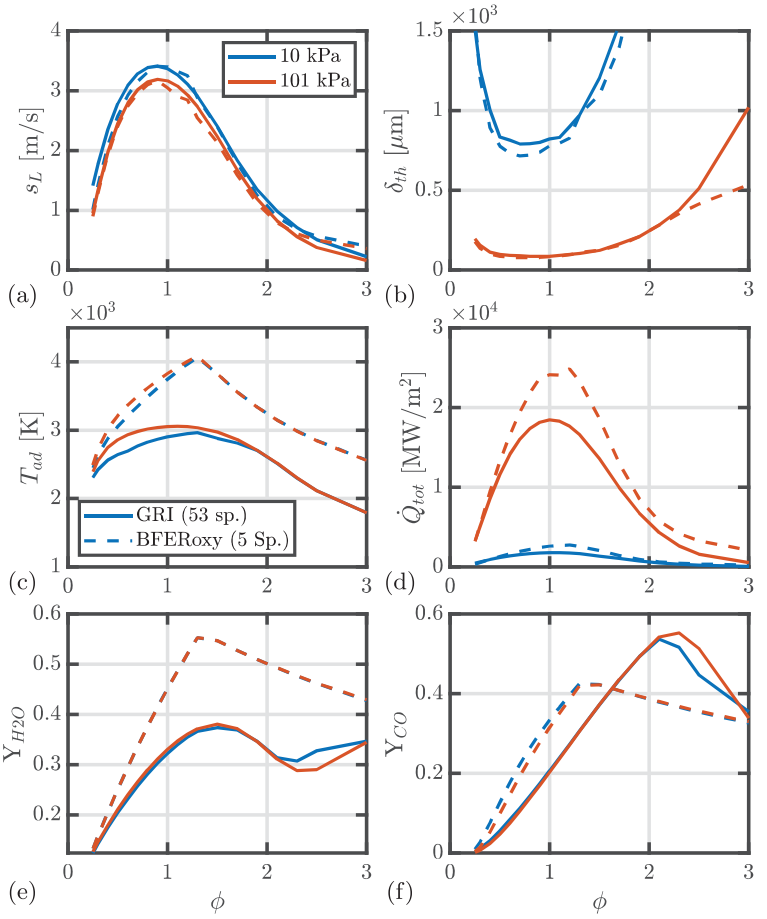

FIGURE 3. Key quantities of 1D premixed oxygen-methane laminar flames with $T_u = 300$ K, as a function of the equivalence ratio ϕ. The quantities shown are (a) the laminar flame speed S_L, (b) the thermal flame thickness δ_{th}, (c) the adiabatic flame temperature T_{ad}, (d) the integrated heat release rate $\dot{Q}_{tot}$ and the burned gas mass fractions (e) Y_{H2O} and (f) Y_{CO}.

The flame speed and flame thickness are well predicted for all equivalence ratios in the range $0.25 < \phi < 3$. Specifically, we note the improvement obtained compared to the results presented in Figure 1 with the existing mechanisms. The maximum error in $\dot{Q}_{tot}$ reaches 40% close to stoichiometry but is minimal for lean and rich conditions. While species concentrations are in good agreement at lean conditions, large errors are present at richer conditions. These differences are likely arise from the lack of radicals (O, H and OH), which are important intermediate species in oxygen-methane combustion.

Finally, the adiabatic flame temperature T_{ad} is grossly overestimated for most conditions investigated. It has to be noted that T_{ad} is solely a function of the species formation enthalpies and heat capacities, and not on the reactions considered. Therefore, the ability of a mechanism to retrieve T_{ad} is only dependent on the species composing the mixture. The BFERoxy mechanism in its current form with five species will have inherent limitations in reproducing the burnt gas state. In the present study, we retain this flawed formulation but note that there are a couple of ways to alleviate this issue. The first

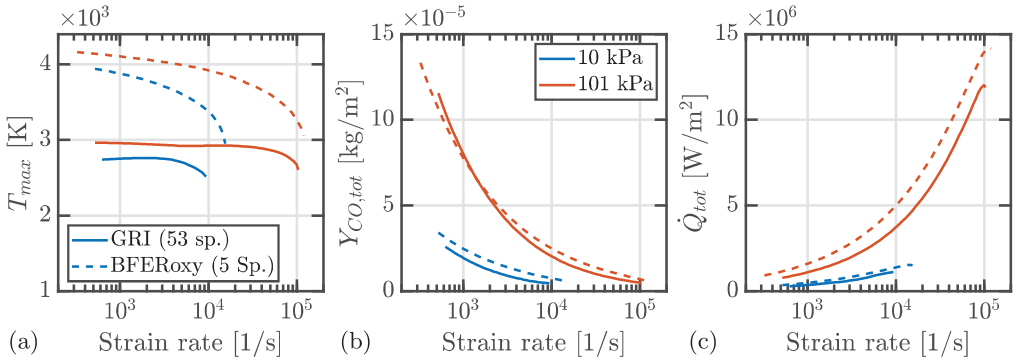

FIGURE 4. Key quantities of 1D counter-diffusion oxygen-methane flames with reactants temperatures $T_u = 300$ K. (a) The maximum temperature T_{max}, (b) the total CO mass $Y_{CO,tot}$, and (c) the total heat release rate $\dot{Q}_{tot}$ are shown as a function of the maximum flow strain rate computed in the domain $\max(\partial u/\partial x)$.

option would be to consider more species, such as radicals. For instance, equilibrium calculations show that including the O and H radicals decreases the T_{ad} error from 800 K to 120 K at the condition $p = 1e5$ Pa, $T_u = 300$ K and $\phi = 1$. The second solution is to alter the thermochemical parameters of the species, for instance, though a data-driven method.

3.2. *Counter-diffusion flames*

1D counter-diffusion flames are used to assess the BFERoxy mechanism performance in a non-premixed configuration. The reactants' temperature was set to $T_u = 300$ K, and the fuel and oxidizer inlet velocities were set to be equal. Solutions were computed for a range of strain rates up to extinction by gradually increasing the inlet velocities. Figure 4 shows the maximum flame temperature T_{max}, the spatially integrated CO $Y_{CO,tot}$ and the spatially integrated heat release rate $\dot{Q}_{tot}$ obtained with the GRI 3.0 and BFERoxy mechanisms.

Similarly to the premixed configuration, T_{max} is overpredicted by the reduced mechanism. The extinction strain rate is also overpredicted by 50% at $p = 10$ kPa, indicating that the flame could be less sensitive to the flow strain. The total mass of CO and heat release are, however, in good agreement between the two mechanisms, suggesting that BFERoxy performs reasonably well in non-premixed configurations.

3.3. *Vortex/premixed flame interaction*

To further assess the strengths and limitations of the BFERoxy mechanism in more realistic configurations, we consider a 2D flame/vortex interaction case. The 2D and 3D computations performed in this study were conducted with the HTR solver (Di Renzo *et al.* 2020) presented in Section 1. For computational cost reasons, the reference solution is performed with the FFCM mechanism. The conditions are taken to be representative of a rocket combustor, as follows: $\phi = 1.6$, $T_u = 300$ K and $p = 30$ kPa. The flow and flame characteristics lead to ratios $u'_{max}/S_L = 6.2$ and $l_{vortex}/\delta_{th} = 4$, where u'_{max} is the maximum velocity fluctuation of the vortex, and l_{vortex} is the vortex core size. By analogy to the turbulent combustion diagram defined by Peters (1999), equating the integral length scale to l_{vortex} and the turbulence intensity to u'_{max}, this configuration

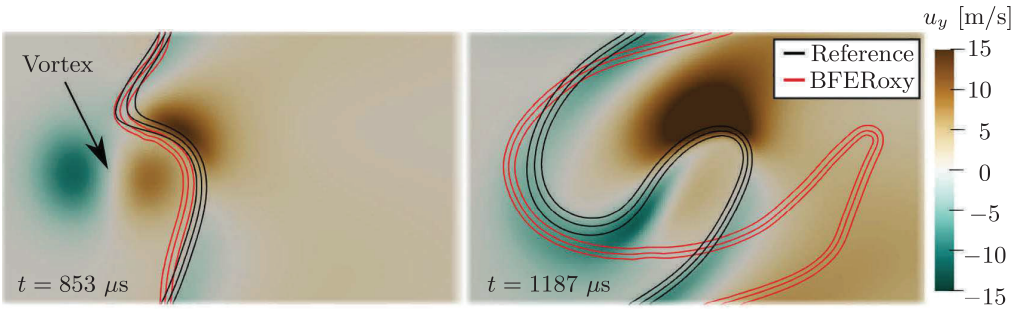

FIGURE 5. (a) Early- and (b) late-stage snapshots of a 2D flame/vortex interaction. The solid lines represent iso-contours 0.25, 0.5 and 0.75 of the dimensionless temperature $\Theta = (T - T_u)/(T_b - T_u)$, while the background represents the transverse velocity.

lies in the thin reaction zone regime, where the reaction zone should remain unaltered and is comparable to a wrinkled laminar flame.

A flow-stabilized laminar flame solution is initialized with a vortex upstream. The vortex is then convected towards the flame, which is distorted by the strain rate of the flow. Figure 5 shows two snapshots, representative of the early and later stages of the interaction. The full lines represent iso-contours of the dimensionless temperature $\Theta = (T - T_u)/(T_b - T_u)$, while the background shows the transverse velocity field. In the early stages, the flame deforms only slightly, and the flame position is similar between the reference mechanism and BFERoxy results. At later stages, however, the flames are strongly distorted, with high flame curvatures, and differences between the two mechanisms are significant.

For more quantitative results about the flame structure, we report in Figure 6 $|\nabla C|$ as a function of C, where $C = (Y_{O2} - Y_{O2,u})/(Y_{O2,b} - Y_{O2,u})$ is the progress variable. Results are shown for the two snapshots displayed in Figure 5, and the red line represents the laminar solution. The laminar solutions are in excellent agreement between the two mechanisms, consistent with the results reported in Sections 3.1 and 3.2. At $t = 853$ μs, both mechanisms lead to a flame that is slightly thinner in some part of the domain. The reference solution possesses flame regions that are more thickened than the semi-global mechanism, but overall most of the flame can be considered laminar. At $t = 1137$ μs, however, the reference flame is significantly thicker than the BFERoxy solution. These differences can be observed in Figure 5, where the flame is subjected to extensive strain, i.e., on the leftmost part of the domain.

Results in Figures 5 and 6 indicate that the semi-global mechanism has a weaker response to large strain rates and/or different nonlinear flame dynamics, i.e., when flame curvature effects alter the local flame speed. These differences are expected based on the differences in extinction strain rates observed in Section 3.2 and have also been reported for the original BFER mechanism for air-methane combustion (Franzelli 2011). In the limit of moderate strain rates, however, the response of the flame modeled with the BFERoxy mechanism is comparable to the reference solution.

3.4. *PSAAP combustor*

In the final test case, we consider the laboratory-scale PSAAP Gas-Gas Model Rocket Combustor (Strelau *et al.* 2023). Gaseous reactants are injected in the chamber through

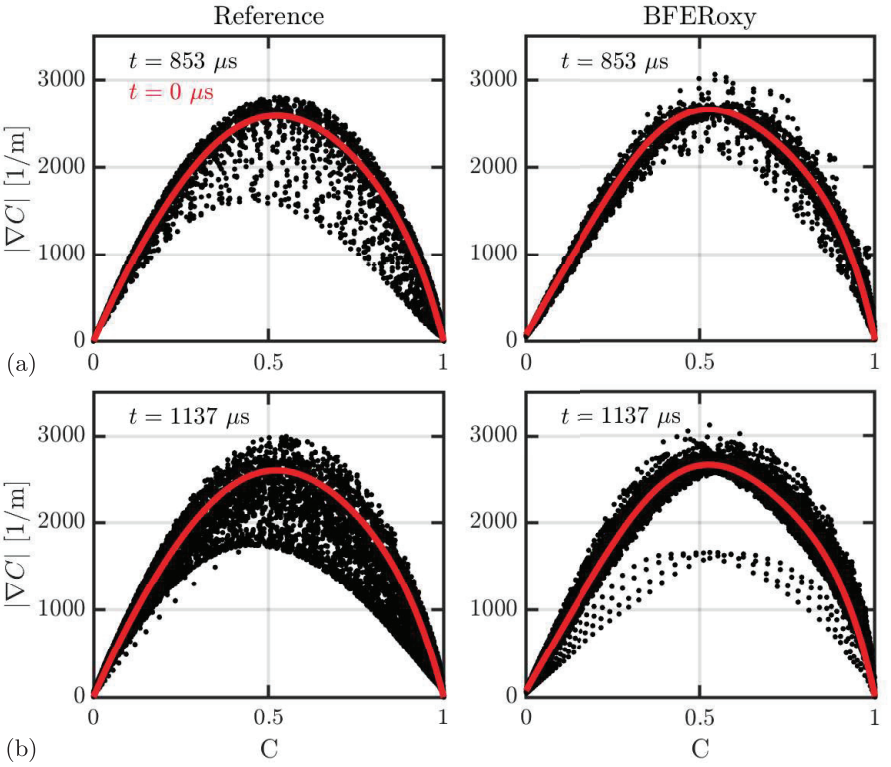

FIGURE 6. 2D flame/vortex interaction comparison with the FFCM and BFERoxy mechanisms at (a) early and (b) late stages of the flame/vortex interaction. The full lines represent iso-contours of temperature, while the color plot shows the transverse velocity field.

an oxygen-centered shear coaxial injector. The laser is deployed for about 7 ns at the jet centerline, which results in an ignition of the reactants roughly 50 μs after deployment. Further details about the configuration and numerical methodology can be found in Wang *et al.* (2021). Figure 7(a,b) shows the equivalence ratio at a plane cutting through the jet, before ignition and after ignition. Even though the reactants are injected in a non-premixed manner, they rapidly mix inside the chamber, resulting in a partially premixed mixture.

Two simulations were performed, one with the FFCM mechanism and one with the BFERoxy model. Figure 8(a,b) displays the mass of water vapor (H_2O) inside the combustor and the maximum temperature T_{max} as a function of the elapsed time from the laser deposition instant. We note a drastic difference in T_{max} between the two simulations, with the semi-global mechanism leading to temperatures up to three times higher. This result is consistent with the overestimation of the adiabatic temperature noted in the previous test cases. A higher T_{max} might lead to two adverse effects. First, a mixture with a higher temperature might ignite faster due to an increased reactivity. Second, the thermal gas expansion will be be stronger, potentially leading to a higher pressure inside the chamber. We analyze these two aspects, as well as the flame kernel development, in the remainder of this section.

The exact ignition time t_{ign}, from which we can assert that the combustor will successfully ignite, is a difficult quantity to define, since the early flame might quench due

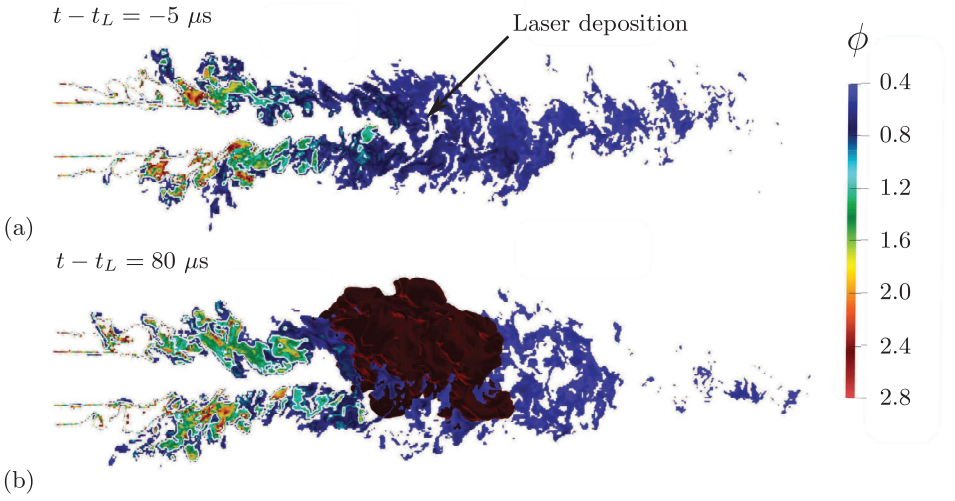

FIGURE 7. Near field of the PSAAP rocket combustor injectors showing the equivalence ratio and the temperature iso-surface corresponding to $T = 1500$ K. Two snapshots are shown: (a) before the laser deposition time t_L and (b) after ignition.

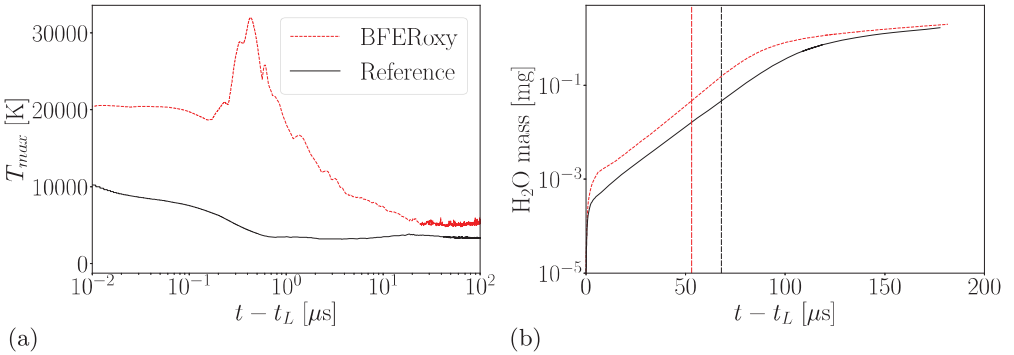

FIGURE 8. Temporal evolution of (a) the water vapor mass inside the combustor and (b) the maximum temperature. The vertical lines in panel (b) represent the ignition time t_{ign}.

to surrounding flow strain rate (Neophytou *et al.* 2012; Esclapez *et al.* 2021). However, the BFERoxy mechanism leads to a slight earlier ignition, since H_2O is produced more quickly. We define t_{ign} to be the instant at which the H_2O mass gets above a threshold, equal to 0.05 mg, which is represented by the vertical lines in Figure 8. While t_{ign} is obviously dependent on the threshold value, the difference in ignition time between the two mechanisms is not, giving us confidence that this method appropriately reflects this ignition delay shift between the two chemistry models.

With this in mind, Figure 9 shows four snapshots comparing the FFCM and BFERoxy results. The black surfaces represent iso-contours of temperature equal to $T = 1500$ K, while the color plot shows the pressure field, normalized by the pre-ignition chamber pressure p_0. The flame kernel development and pressure field are qualitatively very similar between the two simulations, suggesting that the semi-global chemistry adequately retrieves the global flame dynamics of the ignition process. The flame quickly burns the

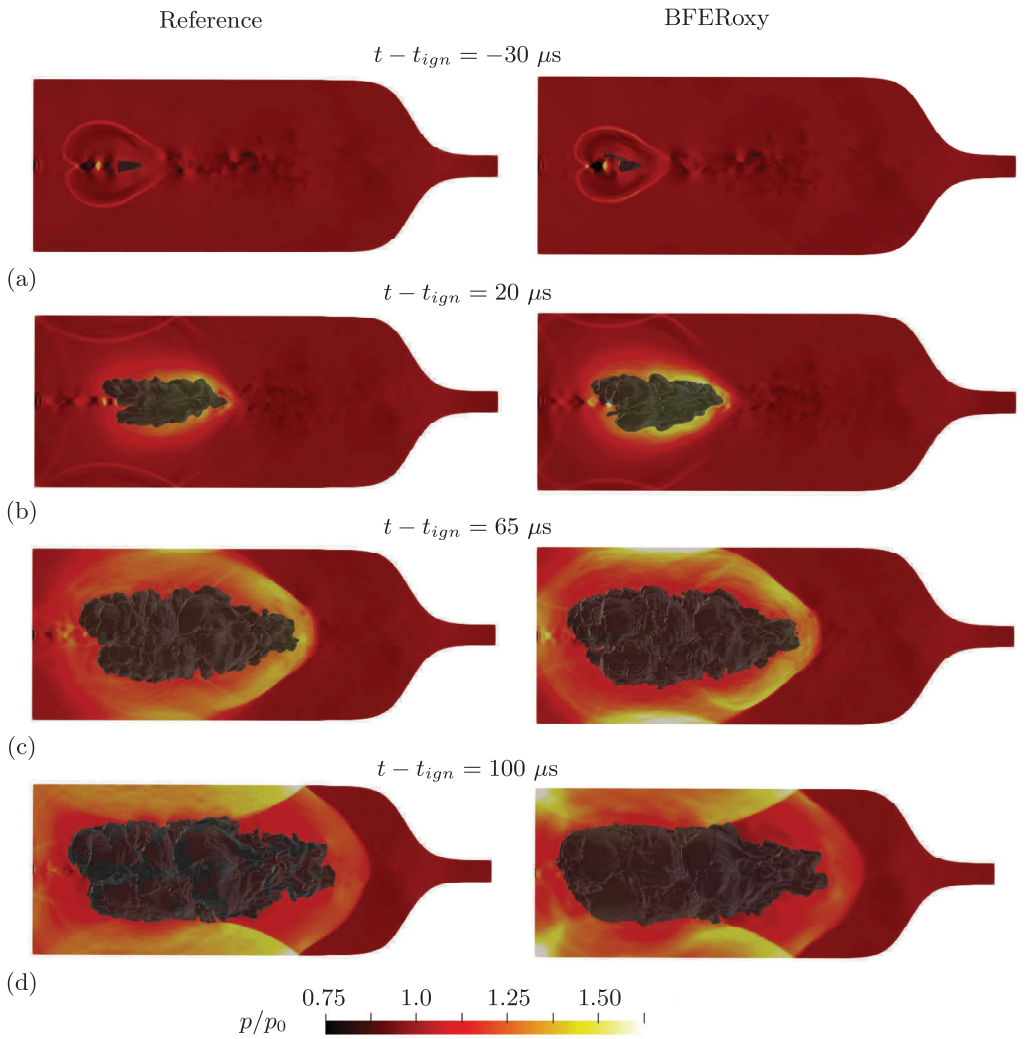

FIGURE 9. Snapshots comparing the PSAAP rocket combustor LES performed with the FFCM and BFERoxy mechanisms. The black surfaces represent iso-contours of temperature equal to $T = 1500$ K, while the color plot shows the pressure field, normalized by the pre-ignition chamber pressure p_0. t_{ign} denotes the ignition time.

surrounding mixed reactants, both upstream and downstream of the laser deposition location. As the flame kernel develops, the pressure inside the combustor rises due to thermal gas expansion.

To analyze this latter aspect more quantitatively, we show in Figure 10 the evolution of the pressure at a probe located at the combustor wall and the average pressure inside the combustor. Both are shown as a function of the time elapsed after t_{ign}. The BFERoxy probe results display a faster rise of the pressure and an overestimation of the peak value, likely due to the higher adiabatic temperature, as discussed earlier. The mean pressure, however, is in excellent agreement between the two simulations, and consistent with the results displayed in Figure 9.

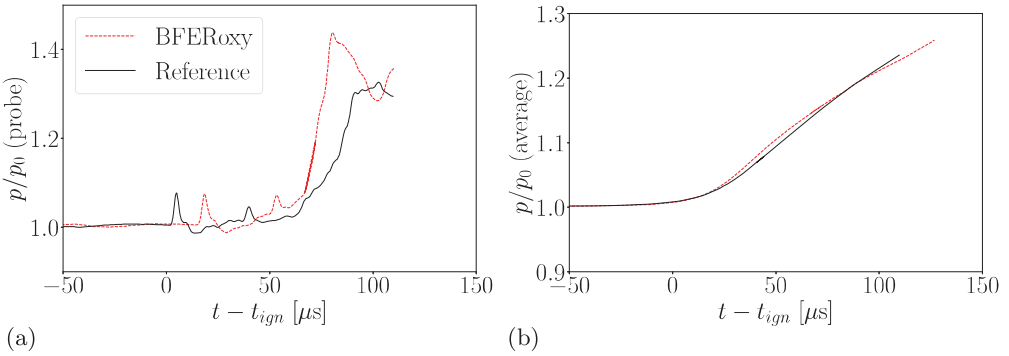

FIGURE 10. Temporal evolution of (a) the pressure at a probe located at the combustor wall and (b) the average pressure inside the combustor.

4. Conclusions

Reducing computational cost and memory load is of paramount importance when performing ensemble, GPU-based computations. To address this issue, we have developed a new semi-global mechanism for oxygen-methane combustion at atmospheric and sub-atmospheric pressure for in-flight ignition of rocket combustors. The semi-global mechanism is a modification of the BFER model from Franzelli *et al.* (2012), featuring five species and two reactions. The chemistry framework retains by design the laminar flame speed and the thermal flame thickness in conditions spanning 0.1 atm $< p <$ 1 atm, 200 K $< T_u <$ 500 K and $0.25 < \phi < 3$. To further assess the performance of the newly devised mechanism, we compared it to reference mechanisms in a range of 1D, 2D and 3D conditions. Overall, the total heat release rate was reasonably predicted, and the response of the flame to moderate strain was comparable to results obtained with more complex mechanisms. However, the mechanism cannot retrieve the adiabatic flame temperature because of the thermochemical properties of the mixture, and flame dynamics under large stretch rates can be significantly different. Application of the BFERoxy mechanism within the PSAAP combustor showed that global features of the ignition and flame kernel development were retained, even though a slightly earlier ignition and local pressure overestimations were observed.

Acknowledgments

This investigation was funded by the U.S. Department of Energy's National Nuclear Security Administration (NNSA) via the Stanford PSAAP-III Center for prediction of laser-induced ignition of rocket engines (Grant Number DE-NA0003968).

REFERENCES

AN, J., HE, G., LUO, K., QIN, F. & LIU, B. 2020 Artificial neural network based chemical mechanisms for computationally efficient modeling of hydrogen/carbon monoxide/kerosene combustion. *Int. J. Hydrogen Energ.* **45**, 29594–29605.

ANDERSEN, J., RASMUSSEN, C. L., GISELSSON, T. & GLARBORG, P. 2009 Global combustion mechanisms for use in CFD modeling under oxy-fuel conditions. *Energ. and Fuels* **23**, 1379–1389.

Brewster, B. S., Cannon, S. M., Farmer, J. R. & Meng, F. 1999 Modeling of lean premixed combustion in stationary gas turbines. *Prog. Energ. Combust.* **25**, 353–385.

CERFACS 2023 *CERFACS Chemical database*, accessed October 2023, https://chemistry.cerfacs.fr/en/chemical-database/mechanisms-list/1-step-methane-air-mechanism/.

Di Renzo, M., Fu, L. & Urzay, J. 2020 HTR solver: An open-source exascale-oriented task-based multi-GPU high-order code for hypersonic aerothermodynamics. *Comput. Phys. Commun.* **255**, 107262.

Esclapez, L., Collin-Bastiani, F., Riber, E. & Cuenot, B. 2021 A statistical model to predict ignition probability. *Combust. Flame* **225**, 180–195.

Franzelli, B. 2011 Impact of the chemical description on direct numerical simulations and large eddy simulations of turbulent combustion in industrial aero-engines. PhD thesis, Institut National Polytechnique de Toulouse.

Franzelli, B., Riber, E., Gicquel, L. & Poinsot, T. 2012 Large eddy simulation of combustion instabilities in a lean partially premixed swirled flame. *Combust. Flame* **159**, 621–637.

Goodwin, D. G., Moffat, H. K. & Speth, R. L. 2018 Cantera: An object-oriented software toolkit for chemical kinetics, thermodynamics, and transport processes.

Heberle, L., Sharma, P. & Pepiot, P. 2021 Automated construction of reduced mechanisms and additive reaction modules. *Combust. Flame* **234**, 111682.

Lu, T. & Law, C. K. 2005 A directed relation graph method for mechanism reduction. *P. Combust. Inst.* **30**, 1333–1341.

Metcalfe, W. K., Burke, S. M., Ahmed, S. S. & Curran, H. J. 2013 A hierarchical and comparative kinetic modeling study of C1−C2 hydrocarbon and oxygenated fuels. *Int. J. Chem. Kinet.* **45**, 638–675.

Neophytou, A., Richardson, E. S. & Mastorakos, E. 2012 Spark ignition of turbulent recirculating non-premixed gas and spray flames: A model for predicting ignition probability. *Combust. Flame* **159**, 1503–1522.

Pepiot-Desjardins, P. & Pitsch, H. 2008 An efficient error-propagation-based reduction method for large chemical kinetic mechanisms. *Combust. Flame* **154**, 67–81.

Peters, N. 1999 The turbulent burning velocity for large-scale and small-scale turbulence. *J. Fluid Mech.* **384**, 107–132.

Sharma, A. J., Johnson, R. F., Moses, A. D. & Kessler, D. A. 2020 Deep learning for scalable chemical kinetics. *AIAA SciTech 2020 Forum, Orlando, FL.* https://doi.org/10.2514/6.2020-0181.

Smith, G., Golden, D. M., Frenklach, M., Moriarty, N., Eiteneer, B., Goldenberg, M., Bowman, C., Hanson, R., Song, S., Gardiner, Jr. W., *et al.* 1999 http://combustion.berkeley.edu/gri-mech/releases.html.

Strelau, R., Frederick, M., Senior, W. C., Gejji, R. & Slabaugh, C. D. 2023 Modes of Laser Spark Ignition of a Model Rocket Combustor. *AIAA SciTech 2023 Forum, National Harbor, MD*. https://doi.org/10.2514/6.2023-2377.

Sun, W., Chen, Z., Gou, X. & Ju, Y. 2010 A path flux analysis method for the reduction of detailed chemical kinetic mechanisms. *Combust. Flame* **157**, 1298–1307.

Tao, Y., Smith, G. P. & Wang, H. 2018 Critical kinetic uncertainties in modeling hydrogen/carbon monoxide, methane, methanol, formaldehyde, and ethylene combustion. *Combust. Flame* **195**, 18–29.

Tomlin, A. S., Pilling, M. J., Turanyi, T., Merkin, J. H. & Brindley, J.

1992 Mechanism reduction for the oscillatory oxidation of hydrogen: Sensitivity and quasi-steady-state analyses. *Combust. Flame* **91**, 107–130.

Wan, K., Barnaud, C., Vervisch, L. & Domingo, P. 2020 Chemistry reduction using machine learning trained from non-premixed micro-mixing modeling: Application to DNS of a syngas turbulent oxy-flame with side-wall effects. *Combust. Flame* **220**, 119–129.

Wang, J., Di Renzo, M., Williams, C. & Iaccarino, G. 2021 Progress on laser ignition simulations of a CH_4/O_2 subscale rocket combustor using a multi-GPU task-based solver. *Annual Research Briefs,* Center for Turbulence Research, Stanford University, pp. 129–142.